Acta Materialia 124 (2017) 343–350

Contents lists available at ScienceDirect

Acta Materialia

journal homepage: www.elsevier.com/locate/actamat

Full length article

Nanoscratching of copper surface by CeO_2

Ning Xu [a], Weizhong Han [a], Yuchun Wang [b], Ju Li [a, c], Zhiwei Shan [a, *]

[a] Center for Advancing Materials Performance from the Nanoscale (CAMP-Nano) & Hysitron Applied Research Center in China (HARCC), State Key Laboratory for Mechanical Behavior of Materials, Xi'an Jiaotong University, Xi'an 710049, China
[b] Anji Microelectronics (Shanghai) Co. Ltd., Shanghai 201203, China
[c] Department of Nuclear Science and Engineering and Department of Materials Science and Engineering, Massachusetts Institute of Technology, 77 Massachusetts Avenue, Cambridge, MA 02139, USA

ARTICLE INFO

Article history:
Received 17 July 2016
Received in revised form
2 November 2016
Accepted 3 November 2016
Available online 16 November 2016

Keywords:
Chemical mechanical planarization
CeO_2 tip
Nanoscratch
Coefficient of friction
Wear

ABSTRACT

CeO_2 nanoparticles based slurries are widely used for chemical mechanical polishing in integrated circuit manufacturing. However, the fundamental processes of material removal and planarization remain elusive. By combining a nanoindenter system with a homemade CeO_2 tip, we investigated the nanoscratching behavior of copper film quantitatively under both constant load and ramp load modes. Based on the evolution of the coefficient of friction, the nanoscratching behavior can be divided into three regimes. For regime I, the coefficient of friction decreases sharply along with the increasing normal load and the copper undergoes mainly elastic deformation. The friction wear begins to enter regime II once the normal load reaches a critical value from where both the coefficient of friction and scratch damage begin to exhibit a changing elastic-plastic characteristic with the increasing of normal load. In regime III, the coefficient of friction reaches a steady value and becomes independent of the normal load and the deformation of copper film enters a steady elastic-plastic state. The coefficient of friction in regime I and II can be well modeled by Hertz contact theory and the classical friction models, respectively. Detailed analysis demonstrates the transition between the two models occurs when the stress concentration approaches the yield strength of copper and the material removal rate can be predicted by adjusting the parameter of the normal force and the abrasive particle size.

© 2016 Acta Materialia Inc. Published by Elsevier Ltd. All rights reserved.

1. Introduction

Chemical-mechanical polishing (CMP) is a standard and ubiquitous method to get local or global planarization on wafers and thin films in IC manufacturing [1–5], such as in the fabrication of the ultra large scale integrated (ULSI) involving shallow trench isolation (STI), inter-level dielectrics (ILD), Cu interconnects, and so on. During CMP, high material removal rates (MRR) and high quality planarization are required in order to achieve a stress-free, defect-free and atomically smooth surface on the wafer. The continuous development of ULSI requires unprecedented surface quality and planarity as the feature size of electronic devices reach the level of nanometers. In order to realize the high MRR and high quality surface planarization, nanoscale particles, such as SiO_2 [6] and CeO_2 [7] are introduced as slurry abrasives. To figure out the mechanism of material removal in CMP several studies have been carried out to investigate the influence of the intrinsic properties of abrasive particles on the polishing effectiveness [8–10]. By employing the fluorescence technology, Luo et al. [11] investigated the real-time particle movement during the CMP. They found that the fixed particles with steady velocity play a leading role for the two body abrasion in CMP material removal. To some extent these results help us understand better the material removal mechanism in CMP. However, because of the wide range of control factors influencing CMP, such as the type of abrasive particles, properties of pad and wafer, chemical environment, down force and rotation speed etc. [11–14], the fundamental mechanisms of the effects of these control factors on polishing performance remains elusive, even though CMP has been extensively adopted in the industry [5,15]. The interaction between abrasive particles and the materials being polished are considered to be one of the key factors controlling the effectiveness of CMP [11–13]. In order to figure out the key parameters that control the effectiveness of CMP while at the same time without being puzzled by the many affecting factors, pure tribology studies had been carried to mimic real CMP process. In addition, the friction and wear introduced by a single particle at

* Corresponding author.
E-mail address: zwshan@mail.xjtu.edu.cn (Z. Shan).

http://dx.doi.org/10.1016/j.actamat.2016.11.008
1359-6454/© 2016 Acta Materialia Inc. Published by Elsevier Ltd. All rights reserved.

the micro- and nano-scale is interesting in its own right for fundamental research of tribology [16,17].

The atomic force microscope (AFM) is the most widely used tool for studying tribology at a fundamental level due to the single-asperity contact between the nanoscale tip and sample [18–20]. It has been employed to study the mechanism of planarization and removal of materials of the single abrasive particle in CMP through nanoscratching [21–25]. In these studies, a nanoscale tip made of silica was used to mimic the friction behavior of single silica particle on various surfaces. Due to high MRR and high selectivity (lager difference of the MRR between two kinds of materials), the CeO_2 nanoparticle based slurries are widely regarded as a typical abrasive [7] for the shallow trench isolation (STI). Methods with the aid of AFM had been also developed to study the planarization and removal of materials by CeO_2 particles. Abiade et al. [26] used a silica AFM tip to scratch the CeO_2 film in order to study the interaction between CeO_2 and silicon. Sokolov et al. [27] studied the interaction behavior of CeO_2 with silica by attaching some CeO_2 nanoparticles to AFM tips. These works advanced the understanding of the mechanism of material removal on silica surface by nanoscale CeO_2 abrasive. However, because that the CeO_2 film cannot represent the properties of the CeO_2 particle [26] and the attached nanoparticles have a great randomness of the morphology and size in polishing process [27], there is a pressing need to develop improved method to reveal the mechanism of the friction and wear by a single scratching particle in a quantitative manner.

In this work, by combining a homemade CeO_2 tip and a TriboIndenter with a 2D transducer, we are able to mimic the mechanical interaction of a single CeO_2 particle with Cu and TEOS (SiO_2) film, respectively. We found that based on the evolution of the coefficient of friction force, the nanoscratching behaviors during the two systems (CeO_2/Cu, CeO_2/SiO_2) both can be divided into three regimes. Because copper is a model material with well-established properties, in this work, we use the nanoscratching of copper film to the homemade CeO_2 tip to demonstrate our findings. The μ in regime I and regime II can be well modeled by Hertz contact theory and the classical friction models, respectively. Detailed analysis demonstrates the transition between the two models occurs when the interior stress concentration approaches the yield strength of copper. Our work is expected to improve the understanding of the mechanism of planarization and removal of material at nanoscale. In addition, the newly developed method in this study can also be employed in exploring other material systems.

2. Materials and experiment set-up

2.1. Preparation of the homemade CeO_2 tip

Preparation process of the homemade CeO_2 tip is shown in the flow diagram of Fig. 1. In order to prepare the bulk sample, the nanoscale CeO_2 particles were synthesized by hydrothermal method at 180 °C for 12 h with $Ce(NO_3)_3$ and KOH as raw materials. From the TEM image (Fig. 1b), it can be seen that the CeO_2 particles with the mean size of 20 nm have polyhedron morphology. Then the CeO_2 nanoparticles were dried and mixed with Polyvinyl Alcohol (PVA, 3%), pulverized and sieved with a 150 μm mesh. Next the green compacts of CeO_2 bulk sample with size of 10 mm in diameter and 2 mm in thickness were formed through compacting under 30 MPa for 10 min, and then the green compacts were sintered at 1200 °C for 2 h in a stainless steel mold. X-ray diffraction was used to confirm the CeO_2 phase in the sintered sample. The microstructure of sintered CeO_2 ceramic was examined by a field emission scanning electron microscope (FESEM, Model: S6600, Hitachi, Japan). As shown in Fig. 1c, micrometer-sized grains are formed in the bulk CeO_2 ceramic. Then the TriboIndenter (TI950, Hysitron, USA) was used to measure the Young's modulus, hardness and roughness of the bulk CeO_2 ceramic and copper film. The hardness of CeO_2 tip is about 7.4 GPa, which is much higher than that of the copper film (1.2 GPa). The ratio of hardness between CeO_2 and copper, i.e., H_{CeO2}/H_{cu} is about 6.2 which is much higher than the critical value (0.7–1.3) [28–30] for generating scratch damage on copper. Therefore, for limited scratching force and distance, CeO_2 tip can be regarded as a rigid particle during the nanoscratching tests.

From Fig. 1a, the sintered sample was then cut into small slices with size of 1 mm × 2 mm × 1 mm and then ground into rods with ~200 μm in diameter and ~1000 μm in length. After careful examinations, one rod was selected and further ground into needle shape with front curvature of ~30 μm. Following this first step, the larger end of the CeO_2 needle was inserted into a metal tip base and glued with organic metal glue manually. To ensure the CeO_2 rod be positioned in the central axis of the tip base, the entire manipulation process was carried out under a stereo microscope. After the glue was fully cured, the tip of the needle CeO_2 was milled into a rectangular pyramid by focused ion beam (FIB, 30 KeV, FEI, USA). By using fine ion beam, the front curvature of the CeO_2 tip can be fabricated as small as ~100 nm. In our study, three different tip radii (120, 180, 270 nm) have been used which are comparable to the particle size used for real CMP process. And one typical example with the tip radius of 180 nm is shown in Fig. 1d and e. Even though the rod used are polycrystalline materials, the top end of the tip is usually a single crystal because of its small size, comparing with the larger average grain size of ~3 μm (Fig. 1c).

2.2. The nanoscratch experiment

The nanoscratch experiment setup is shown schematically in Fig. 2a. The scratch tests were carried out in both ambient and dry atmosphere (humidity less than 5%, dry by silica gel desiccant for 12 h) by using TI 950 TriboIndenter with a 2D transducer, which can yield high precision displacement and force data in both normal and lateral directions. The copper film used in this work was deposited on a commercial blank silicon wafer with the stack of Cu/Ta/TaN/SiO_2/Si and the Cu thickness is 1.5 μm. For each data point, five repeated experiments were performed to reduce the test errors. A SEM was used to observe the scratch morphologies of copper and the CeO_2 tip after the scratch tests. Both ramp (the normal force increases from 0 at a constant rate during the whole scratch process) and constant (the normal force maintain constant during the scratch process) load modes were used. The scratch length was set to be 8 μm and the normal force ranged from 0 μN to 300 μN. As shown in Fig. 2b and c, each scratch experiment procedure of CeO_2 tip on copper film surface is composed of 3 steps. Firstly, a prescan with a constant normal force of 2 μN was performed to get the initial surface information (height and roughness) of the tested sample which will be used to correct the final scratch depth and residual depth (named tilt correction). Then, the tip turned back and scratched the copper film with 0.5 μm/s. The normal load increased from 0 to 300 μN uniformly for ramp mode and maintained a constant for constant mode. Finally, a postscan of the tip with a normal force of 2 μN was carried out to get residual depth information of the scratch.

3. Results

3.1. Variation of the scratch depth during the scratch experiment under ramp force mode

Five scratch tests were carried out in total under ramp load

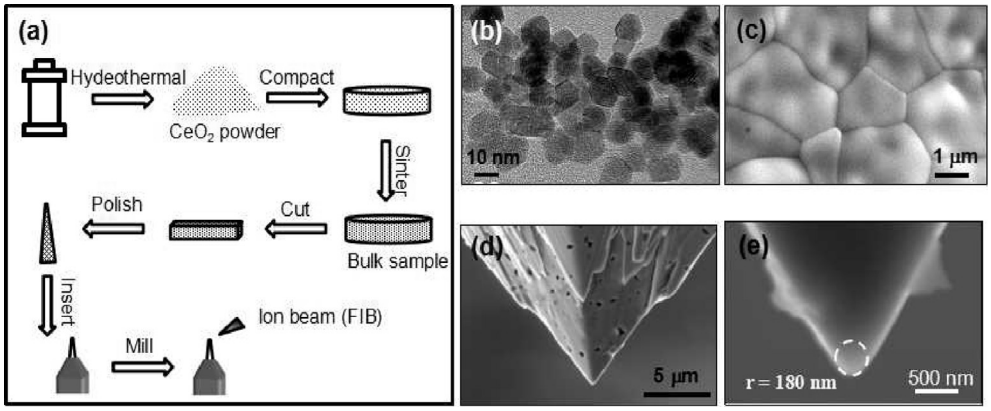

Fig. 1. The synthesis of CeO_2 tip and setup of the nanoscratch experiment. (a) Flow diagram of the preparation process of homemade CeO_2 tip. (b) TEM image of the CeO_2 nanopowders synthesized by hydrothermal method. (c) SEM image of microstructure of the sintered CeO_2 bulk material. (d) SEM image of the rectangular pyramid shape of CeO_2 tip milled by focus ion beam. (e) Enlarged SEM image of the CeO_2 tip with a front radius of 180 nm.

mode. For each test, the force was programed to increase from 0 to 300 μN when the scratch distance increases from 0 to 8 μm. Despite some small differences, the measured coefficient of friction (COF, μ, defined as the ratio of the friction force divided by the normal force during the scratch) always exhibits three distinctive stages. One typical example is shown in Fig. 3. The variation of scratch depth (after tilt correction) as a function of the lateral displacement are plotted in Fig. 3a. The small fluctuation of the curve indicates that the sample surface is relatively smooth. And the scratch depth increases near linearly with the normal force, and achieves maximum depth of ~280 nm at normal force of 300 μN (pink data, Fig. 3a). Finally, the postscan was programed to measure the residual depth of the scratch. The maximum residual depth is ~180 nm which means the elastic recovery of the copper film is about 100 nm when a normal force of 300 μN was released. The inserted SEM image in Fig. 3a displays the morphology of the scratch. No detectable plastic deformation can be found when the normal force is less than 15 μN. Following this, the scratch becomes deeper and wider along with increasing normal forces. The extruded copper piles up along the scratch and reach a maximum height of ~180 nm at the end of the scratch, as measured by the postscan curve in Fig. 3a.

3.2. Variation of the normal force and coefficient of the friction force during the scratch experiment under ramp force mode

The normal force and friction force as a function of the lateral displacement is shown in Fig. 3b. As programed, the normal force increase linearly with the increasing lateral displacement (black data, Fig. 3b). However, it is interesting to note that the friction force (blue data, Fig. 3b) first increases linearly with increasing lateral displacement (Regime I in Fig. 3b) but elevates its linear slope suddenly when the lateral displacement reaches a value of ~2 μm. Following this, the friction force increases in a serrated manner, presumably due to stick-slip behavior [31,32] and polycrystalline nature of the copper film (the friction properties can be affected by grain boundaries and crystal orientation). Fig. 3c displays the variation of the calculated coefficient of friction force (μ) with the increasing of applied normal load. It is obvious that the μ demonstrates three distinct stages (Fig. 3c). With the increasing normal force, the μ quickly decreases from ~1.6 to ~0.2 in stage I, increases from 0.2 to ~0.9 in stage II and then fluctuates around ~0.9 in regime III. The observed three friction stages agrees well with the adhering, ploughing and cutting regimes described by previous molecular dynamic simulations [33,34]. To our best knowledge, this is the first experimental report on observing all three friction regimes in a single nanoscratching experiment.

3.3. Variation of the scratch depth and coefficient of friction force during the scratch experiment under constant force mode

In order to confirm the observed three stage frictions are universal phenomena instead of accidental and also to mimic the constant down-force condition in CMP, we performed a series of scratch experiments in constant load mode also, i.e. the normal force is kept unchanged during the scratch test. One of the tests with normal force 150 μN is shown in Fig. 4a. Under constant load mode, scratch depth and residual depth remain almost constant, as supported by the post-test morphology of the scratch (SEM image in Fig. 4a inset).

The fluctuations of the depth should result from the anisotropic grains of the copper film. The summarized evolution of μ vs. normal force is plotted in Fig. 4b. Each data point represents an average of five sets of experiments under the same normal load condition. It is obvious that the μ also demonstrates three characteristic friction stages, which is consistent with the results achieved under ramp load mode.

3.4. Variation of scratch depth, residue depth and elastic recovery rate with the increasing of normal force

In order to acquire a quantitative understanding of the three stages of friction coefficient, we have summarized the scratch depth vs. residual depth data and plotted them in Fig. 5a. Again, each data point represents the average of five repeated scratches. And it is obvious that the rising rate of the residual depth is lower than that of the scratch depth along with the increasing normal force. The difference between scratch depth and residual depth is the magnitude of elastic recovery, and the ratio between elastic recovery value and scratch depth is defined as the elastic recovery ratio. Fig. 5b shows the variation of elastic recovery ratio as a function of the normal force. It is interesting that the curve of elastic recovery ratio can also be divided into three stages, which matches with the variation of μ with normal force shown in Figs. 3c and 4b. Despite the large scattering of the data, stage I demonstrated mainly elastic deformation, and has close to 100% elastic recovery ratio. Once the normal force passed the first critical point (about 15 μN in this work) the elastic recovery ratio decreased quickly in stage II and reached a plateau of 45% when the normal force reaches the second critical point (about 80 μN in this work).

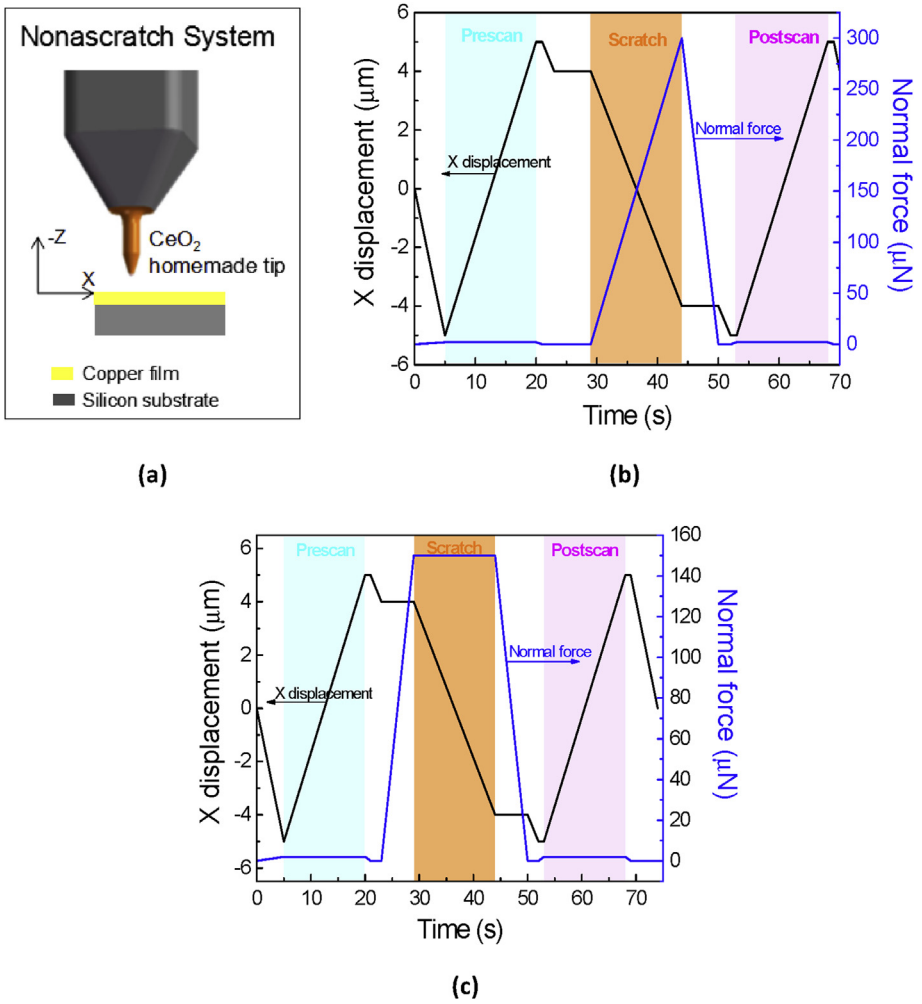

Fig. 2. The set-up of the nanoscratch experiment. (a) Setup of the nanoscratch experiment with the nanoindenter. (b) The load function of the scratch experiment of the ramp mode. (c) The load function of the scratch experiment under constant mode.

4. Discussion

4.1. The elastic dominated deformation of the copper film during the nanoscratching

From above we can see that the variation of elastic recovery ratio of copper film with normal force during the scratch process indicates that there is a direct relationship between deformation character and the tribology properties. The stage I, II and III of coefficient of friction force corresponds to elastic, changing elastic-plastic and steady elastic-plastic dominated deformation, respectively. The fast removal of materials in CMP is suggested to be performed in stage II due to the tunable μ and relatively gentle scratch. It might be possible to planarize materials in an atom-by-atom removal ('atomic attrition') mode [35] in stage I also, if previous damage has occurred on copper surface.

Our test was carried out in room environment. A mixture of Cu oxide and adsorption layers can be formed on the surface of copper (as illustrated in Fig. 6a), which may likely influence the friction behaviors. The thickness of the top adsorption layer is mainly affected by the air humidity. In order to minimize its effect, we purposely controlled the relative humidity of the testing chamber to be less than 5% by placing dryer (silica gel desiccant) inside the chamber for 12 h before the test. In addition, cross-sectional view TEM examination confirmed that the Cu oxide layer is only around a few nanometers, similar to that reported by Wheeler et al. [36]. Considering the force used in our study is well above μN, the influence of Cu oxide and adsorption layer can be ignored in this study.

In stage I, the copper mainly undergoes elastic deformation (Fig. 5b) and the front end of the CeO_2 tip could be considered as a rigid sphere due to its high hardness. Therefore, it is reasonable to consider the contact between the CeO_2 tip and copper film them as Hertzian elastic contact. As illustrated in Fig. 6b, the radius of the front end of the tip is marked as r, the normal force is F_n, the friction force is F_f, the scratch depth is h and the contact radius is a. The friction force in stage I is believed to be the breaking of adhesion junctions between the CeO_2 tip and the top surface of copper film [18,37,38]. According to the theory of the Leonard and Amontons [39], the friction force introduced by adhesion can be expressed as:

$$F_f = \tau_a A_a \tag{1}$$

where τ_a is the adhesion shear strength between copper film and CeO_2 tip, A_a is the contact area between tip and copper film. The contact area between the tip and copper film can be expressed by the Hertz elastic solution [40]:

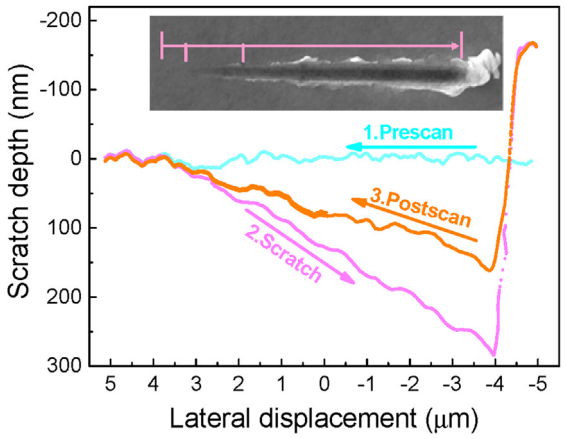

(a)

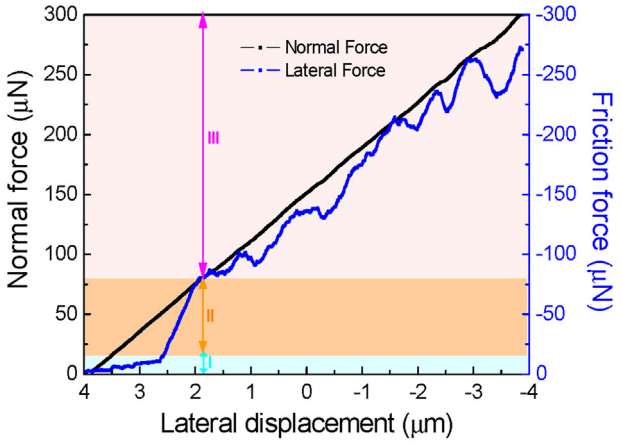

(b)

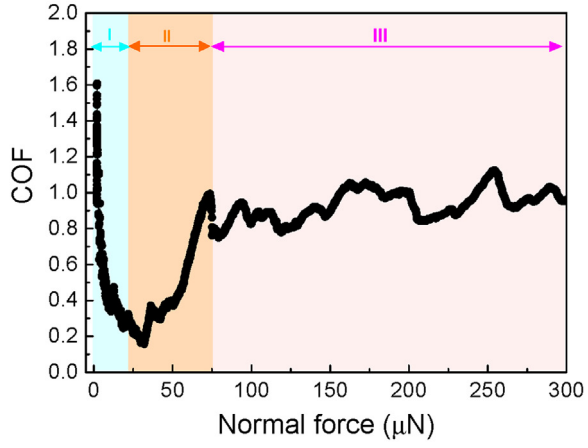

(c)

Fig. 3. Variation of scratch depth, normal force, friction force and coefficient of the friction force during the scratch experiment under ramp force mode. (a) Scratch depth as a function of lateral displacement of the ramp mode. Inserted SEM image illustrates the scratch morphology under ramp mode. (b) Normal force and friction force during the scratch as a function of the lateral displacement. (c) Coefficient of the friction force as a function of the normal force of ramp force mode.

$$A_a = \pi(r/K \cdot F_n)^{2/3} \tag{2}$$

where

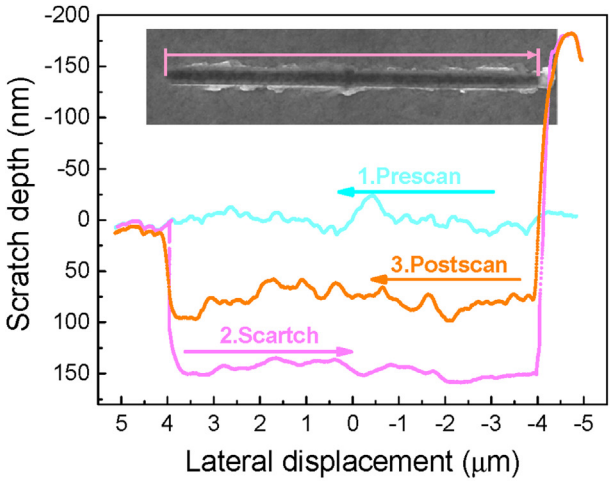

(a)

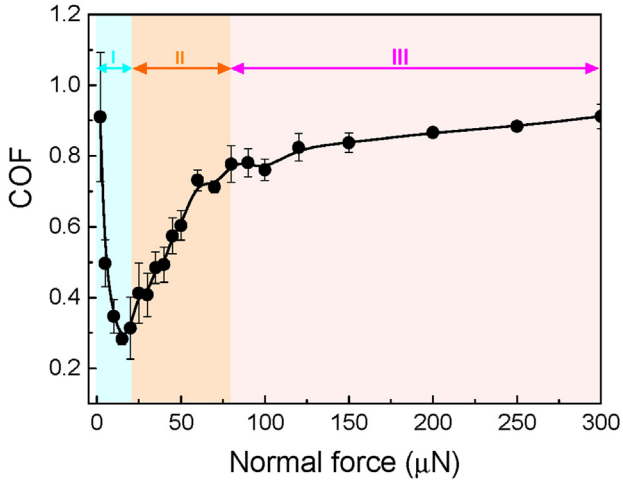

(b)

Fig. 4. Variation of scratch depth and coefficient of friction force during the scratch experiment under constant mode. (a) Scratch depth as a function of the lateral displacement of the constant force mode, the inset SEM image illustrates the scratch morphology with normal force of 150 μN. (b) Coefficient of the friction force as a function of the normal force of the constant force mode.

$$K = 4/3 \cdot \left(\left(1-\upsilon_1^2\right)/E_1 + \left(1-\upsilon_2^2\right)/E_2\right)^{-1} \tag{3}$$

and the E_1, ν_1, E_2, ν_2 are the elastic moduli and Poisson's ratios of CeO_2 tip and copper film, respectively. Therefore the variation of μ with applied normal force in stage I can be expressed as:

$$\mu_a = F_f/F_n = \tau_a \pi (r/K)^{2/3} F_n^{-1/3} \tag{4}$$

According to the measured values (using Hysitron TI950) for E_1, E_2, ν_1, ν_2, (62.4 GPa, 66.5 GPa, 0.3 and 0.35) and Equation (4), μ_a decreases with increasing normal force in stage I, consistent with the measurement shown in Figs. 3c and 4b. By letting $\tau_a = 1.05$ GPa, Equation (4) can depict the variation of μ with the normal force in stage I very well, as plotted in Fig. 6d with blue color. Usually the adhesion strength (τ_a) is only depending on the contacted materials [18,41,42], and the estimated value of ~1.05 GPa is in the typical range of the adhering shear strength [43–46]. Therefore, the

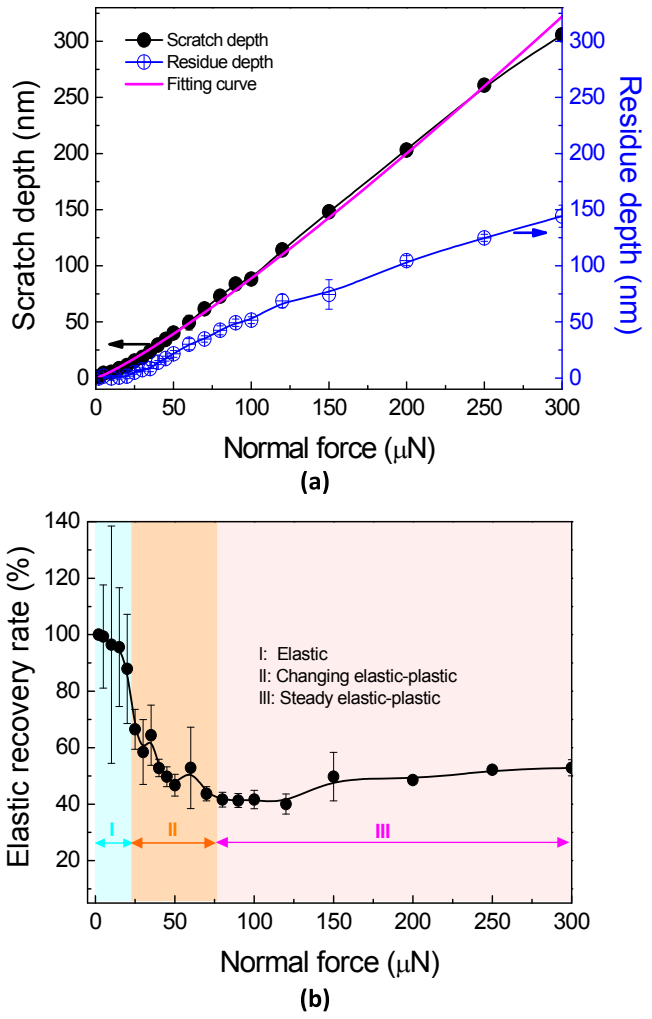

Fig. 5. Variation of scratch depth, residue depth and elastic recovery rate with the increasing of normal force. (a) Scratch and residue depth as a function of normal force under constant force mode. (b) Elastic recovery rate as a function of normal force during the scratch under constant force mode.

current experimental method likely can be used as a procedure to measure the interfacial shear strength between two materials.

4.2. The elastic-plastic and steady plastic dominated deformation of the copper film during the nanoscratching

Once the applied normal force becomes larger than the first critical point, μ increases sharply while at the same time the elastic recovery rate continuously decreases with the increasing normal force until the normal force reaches 80 μN in this work (Figs. 4b and 5b). In addition, more and more wear debris and material pileup begin to be produced in this stage, as shown by the SEM image in Fig. 3a. The interaction between the CeO_2 spherical tip and copper film in stage II is illustrated in Fig. 6c. *A* and *S* are the projected area of the contact in lateral direction and normal direction, respectively. The geometric relationship of the parameters is expressed in the lower right part of Fig. 6c. According to the Bowden-Tabor model [41], the coefficient of friction in the ploughing regime can be expressed as:

$$\mu_p = F_f \Big/ F_n = (\tau_p A)/(\sigma_p S) \tag{5}$$

where τ_p and σ_p are the stress in horizontal and vertical orientation on the copper film during the scratching, respectively. According to the geometric relationship described in Fig. 4c, the variation of μ_p in changing elastic-plastic regime can be derived as:

$$\mu_p = 4/3 \cdot \tau_p \Big/ \sigma_p \cdot \pi\sqrt{2\lambda - \lambda^2} \tag{6}$$

where λ is the ratio of scratch depth (h) over the tip radius (r), and h is a function of the applied normal force ($h = 0.533F_n^{1.12} - 2.057$, as fitted in Fig. 5a). According to Equation (6), the fitting curve of μ as a function of the normal force in stage II is plotted in Fig. 6d with red color. By letting $\tau_p/\sigma_p = 2.2$, the red curve yielded from Equation (6) shows an excellent agreement with the experimental data. $\tau_p = 2.2\sigma_p$ indicate that the tip requires more force to set it in motion in the horizontal direction during the nanoscratching, which is why the μ increases sharply in the second regime. This is probably due to the necessity to plastically deform and displace the materials surrounding the tip in addition to breaking the interfacial shear strength, in order to move horizontally.

So far, both stage I and II can be described well by two different models, as shown in Fig. 6d. And the blue curve and red curve show a good agreement with the experiment results in the adhering and ploughing regime, respectively. In addition, the curves predicted by these two models do cross each other at which the applied normal

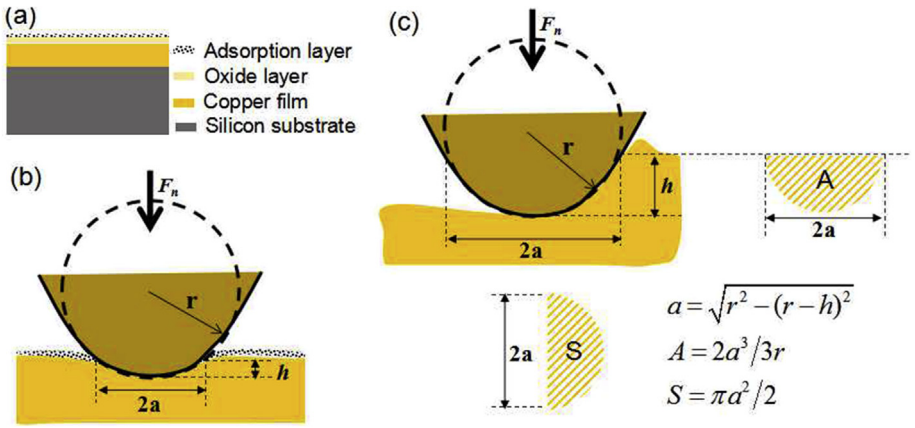

Fig. 6. Schematic illustration of the contact between CeO_2 tip and copper under adhering and ploughing friction. (a) The illustration of the likely topmost layer structure of adsorption and oxide layer in copper. (b) Schematic of the cross-section view of the spherical tip and elastic semi-plane under adhering friction. (c) Schematic of spherical tip and contact condition between the tip and copper film during the ploughing friction. (d) Calculated COF as a function of the normal force for adhering and ploughing friction.

stress at the point for transition from elastic to changing elastic-plastic regime stress is about 1.6 GPa, which is close to the yielding strength of copper under nanoindentation (H = 1.4 GPa). That is to say, Equation (4) and Equation (6) can be used to predict the general trend of the variation of COF as a function of the normal force in the elastic deformation and elastic-plastic deformation of the copper during micronano scale scratch, respectively.

Once the normal force higher than 80 μN in this system, the cutting friction takes over. In this regime, the friction force increases linearly with the applied normal force, as shown in Figs. 3b, c and 4b. The μ keeps constant, which is consistent with Amontons' 1st Law [47]. This result is also in agreement with the experimental results obtained by Bull et al. [48–50]. Interestingly, the elastic recovery ratio of the copper in cutting friction also remains stable as shown in Fig. 5b.

According to the distinct character of three stages, we suggest that, the elastic and changing elastic-plastic regimes are proper wear regimes that should be used in CMP removal process because of the effectively materials removing, tunable μ and relatively gentle scratches. The variation of μ in this regime can be well described by models, which means the material removal rate can be predicted before CMP via adjusting the parameter of the normal force (F_n) and the particle size (r) during the real application. The current investigations pave the way to study the friction mechanism of a single abrasive particle to the flat surface and the effect of the normal force on friction at the nanoscale.

The elastic-plastic deformation characteristics of copper as well as the evolution of the COF during the scratch tests are expected to be close related to dislocation-mediated plasticity. However, despite of some pioneering efforts [51–56], it remains a puzzle with regard to the quantified relationship between these factors. It is our plan next to clarify this through performing systematic studies on the residual dislocation structures of scratches under different loading conditions.

5. Conclusions

In conclusion, a new method to study the mechanism of friction and wear of a single particle at nanoscale is established. The friction processes of the CeO_2 tip and copper can be divided into three stages (elastic, changing elastic-plastic and steady elastic-plastic) according to the variation of μ and deformation of copper. Nearly elastic deformation of the copper plays the dominant role and μ is negatively correlated with the normal force in regime I. When the normal force exceeds the first critical normal force, the yield strength of the copper, the elastic-plastic transformation of copper occurs and the changing elastic-plastic dominated deformation takes place, then μ increases sharply with increasing normal force. Once the normal force exceeds the second critical value, the deformation of the copper and the μ both remain stable. Our findings suggest that an optimal condition of planarization and removal of material in CMP should be set within the regime I to reduce the wafer surface to sub-nanometer scale roughness, and regime II to accomplish high material removing rate with relatively gentle scratches, respectively. The mechanism of planarization and removal of other materials, such as the TEOS, Si_3N_4 and so on, used in semiconductor industry and the size effect of the tip radius on nanoscratching behaviors will be further investigated by this method in the future.

Acknowledgements

This work was supported by the grants from NSFC (50925104, 51471128, 51231005, and 51321003) and 973 Program of China (2010CB631003, 2012CB619402). We also appreciate the support from the 111 Project of China (B06025). W.Z.H. would like to thank the support of Youth Thousand Talents Program of China and the Young Talent Support Plan of XJTU. J.L. acknowledges support by NSF DMR-1120901. N.X. acknowledges S.L.Z. and J.X.Z. for their assistance in scratch experiments.

References

[1] J.M. Steigerwald, S.P. Murarka, R.J. Gutmann, D.J. Duquette, Chemical process in the chemical-mechanical polishing of copper, Mater. Chem. Phys. 41 (1995) 217–228.
[2] F.G. Shi, B. Zhao, Modeling of chemical-mechanical polishing with soft pads, Appl. Phys. A Mater. 67 (1998) 249–252.
[3] R.K. Singh, S.M. Lee, K.S. Choi, B.G. Bahar, W. Choi, Z. Chen, B.M. Moudgil, Fundamentals of slurry design for CMP of metal and dielectric materials, MRS Bull. 27 (2002) 752–760.
[4] C. Wonseop, U. Mahajan, L.S. Maha, J. Abidae, R.K. Singh, Effect of slurry ionic salts at dielectric silica CMP, J. Electrochem. Soc. 151 (2004) G185–G189.
[5] P.B. Zantye, A. Kumar, A.K. Sikder, Chemical mechanical planarization for microelectronics applications, Mater. Sci. Eng. R. 45 (2004) 89–220.
[6] J.A. Levert, C.S. Korach, CMP friction as a function of slurry silica nanoparticle concentration and diameter, Tribol. T 52 (2009) 256–261.
[7] X.D. Feng, D.C. Sayle, Z.L. Wang, M.S. Paras, B. Santora, A.C. Sutorik, T.X.T. Sayle, Y. Yang, Y. Ding, X.D. Wang, Y.S. Her, Converting ceria polyhedral nanoparticles into single-crystal nanospheres, Science 312 (2006) 1504–1508.
[8] G.R. Abrahamson, E.J. Duwell, W.J. McDonald, Wear and lubrication as observed on a lap table with loose and bonded abrasive grit, J. Tribol. T Asme 113 (1991) 249–254.
[9] J.L. Basse, H. Liang, Probable role of abrasion in chemo-mechanical polishing of tungsten, Wear 233 (1999) 647–654.
[10] D.C. Mejia, S.A. Beaudoin, Locally relevant prestonian model for wafer polishing, J. Electrochem. Soc. 150 (2003) G96–G102.
[11] J. Lei, D. Guo, J. Luo, G. Pan, Probing particle movement in CMP with fluorescence technique, J. Electrochem. Soc. 158 (2001) H681–H685.
[12] L.M. Cook, Chemical processes in glass polishing, J. Non Cryst. Solids 120 (1990) 152–171.
[13] I.R. Kramer, L.J. Demer, Effects of environment on mechanical properties of metals, Prog. Mater. Sci. 9 (1961) 133–199.
[14] J.T. Abiade, W. Choi, R.K. Singh, Effect of pH on ceria-silica interactions during chemical mechanical polishing, J. Mater. Res. 20 (2005) 1139–1145.
[15] W. Choi, S.M. Lee, J. Abiade, R.K. Singh, Estimation of fractional surface coverage of particles for oxide CMP, J. Electrochem. Soc. 151 (2004) G368–G372.
[16] S. Islam, R.N. Ibrahim, Mechanism of abrasive wear in nanomachining, Tribol. Lett. 42 (2001) 275–284.
[17] Y.W. Zhao, L. Chang, A micro-contact and wear model for chemical-mechanical polishing of silicon wafers, Wear 252 (2002) 220–226.
[18] S. Izabela, C. Michael, W.C. Robert, Recent advances in single-asperity nanotribology, J. Phys. D Appl. Phys. 41 (2008) 1–39.
[19] W.C. Robert, Scratching the surface:fundamental investigations of tribology with atomic force microscopy, Chem. Rev. 97 (1997) 1163–1194.
[20] E. Gnecco, R. Bennewitz, T. Gyalog, E. Meyer, Friction experiments on the nanometer scale, J. Phys. Condens. Matter 13 (2001) R619–R942.
[21] W.A. Ducker, T.J. Senden, R.M. Pashley, Direct measurement of colloidal forces using an atomic force microscope, Nature 353 (1991) 239–241.
[22] Y.Q. Li, N.J. Tao, J. Pan, A.A. Garcia, S.M. Lindsay, Direct measurement of interaction forces between colloidal particles using the scanning force microscope, Langmuir 9 (1993) 637–641.
[23] I. Sokolov, Q.K. Ong, H. Shodiev, N. Chechik, D. James, M. Olier, AFM study of forces between silica, silicon nitride and polyurethane pads, J. Colloid Interface Sci. 300 (2006) 475–481.
[24] B. Bhushan, J.N. Israelachvili, U. Landman, Nanotribology: friction, wear and lubrication at the atomic-scale, Nature 374 (1995) 607–616.
[25] Y. Mo, W. Zhao, M. Zhu, M. Bai, Nano/microtribological properties of ultrathin functionalized imidazolium wear-resistant ionic liquid films on single crystal silicon, Tribol. Lett. 32 (2008) 143–151.
[26] J.T. Abiade, S. Yeruva, W. Choi, B.M. Moudgil, D. Kumar, R.K. Singh, A tribochemical study of ceria-silica interactions for CMP, J. Electrochem. Soc. 153 (2006) G1001–G1004.
[27] Q.K. Ong, I. Sokojov, Attachment of nanoparticles to the AFM tips for direct measurements of interaction between a single nanoparticle and surfaces, J. Colloid Interf. Sci. 310 (2007) 385–390.
[28] M.S. Ding, W.Z. Han, J. Li, E. Ma, Z.W. Shan, In situ study of the mechanical properties of airborne haze particles, Sci. China 58 (2015) 2046–2051.
[29] M.M. Khruschov, Principles of abrasive wear, Wear 28 (1974) 69–88.
[30] W.Z. Han, L. Huang, S. Ogata, H. Kimizuka, Z.C. Yang, C. Weinberger, Q.J. Li, B.Y. Liu, X.X. Zhang, J. Li, E. Ma, Z.W. Shan, From "smaller is stronger" to "size-independent strength plateau": towards measuring the ideal strength of iron, Adv. Mater. 27 (2015) 3385–3390.
[31] M.H. Cho, S.J. Kim, D.S. Lim, H. Jang, Atomic scale stick-slip caused by dislocation nucleation and propagation during scratching of a Cu substrate with a nanoindenter: a molecular dynamics simulation, Wear 259 (2005)

1392–1399.
[32] M. Feldmann, D. Dietzel, A. Tekiel, J. Topple, P. Grutter, A. Schirmeisen, Universal aging mechanism for static and sliding friction of metallic nanoparticles, Phys. Rev. Lett. http://dx.doi.org/10.1103/Phy Rev Lett.117.025502.
[33] L.C. Zhang, H. Tanaka, Towards a deeper understanding of wear and friction on the atomic scale - a molecular dynamics analysis, Wear 211 (1997) 44–53.
[34] L.C. Zhang, K. Mylvaganam, Nano-tribological analysis by molecular dynamics simulation - a review, J. Comput. Theor. Nanosci. 3 (2006) 167–188.
[35] T.D.B. Jacobs, R.W. Carpick, Nanoscale wear as a stress-assisted chemical reaction, Nat. Nanotechnol. 8 (2013) 108–112.
[36] D.R. Wheeler, Effect of adsorbed chlorine and oxygen on the shear strength of iron and copper junctions, J. Appl. Phys. 477 (1976) 1507–1531.
[37] E. Rabinowicz, Friction and Wear of Materials, John Wiley, New York, 1965.
[38] F.P. Bowden, D. Tabor, Friction and Lubrification, Revised Edition, London, New York, 1967.
[39] B. Bhushan, Modern Tribology Handbook, CRC Press, Boca Raton, 2001.
[40] K.L. Johnson, One hunderd years of Hertz contact, Tribol. Group Namin. Lect. 196 (1981) 363–378.
[41] Y.J. Mergler, R.J. Kampen, W.J. Nauta, R.P. Schaake, B. Raas, J.G.H. Griensver, G.J.M. Meesters, Influence of yield strength and toughness on friction and wear of polycarbonate, Wear 258 (2005) 915–923.
[42] H.S. Benabdallah, Static friction coefficient of some plastics against steel and aluminum under different contact conditions, Tribol. Int. 40 (2007) 64–73.
[43] E. Meyer, Site-specific friction force spectroscopy, J. Vac. Sci. Technol. B 14 (1996) 1285–1288.
[44] J. Roster, M. Baker, H. Harders, Mechanical Behaviour of Metals, Springer Berlin Heidelberg, 2007, pp. 162–225.
[45] G. Dehm, M. Ruhle, H.D. Conway, R. Raj, A microindentation method for estimating interfacial shear strength and its use in studying the influence of Titanium transition layers on the interface strength of epitaxial copper films on sapphire, Acta Mater. 45 (1997) 489–499.
[46] J. Wang, R.G. Hoagland, J.P. Hirth, A. Misra, Atomistic simulations of the shear strength and sliding mechanisms of copper-niobium interfaces, Acta Mater. 56 (2008) 3109–3119.
[47] H.H. Gowell, J. Mazur, Amonton's law and fiber friction, J. Text. Inst. 44 (1953) 59–69.
[48] S.J. Bull, D.G. Bhat, M.H. Staia, Properties and performance of commercial TiCN coatings. Part 2: tribological performance, Surf. Coat. Technol. 163–164 (2003) 507–514.
[49] S.J. Bull, E.G. Berasetegui, An overview of the potential of quantitative coating adhesion measurement by scratch testing, Tribol. Int. 39 (2006) 99–114.
[50] J.J. Chen, Z.S. Lin, B.J. Bull, C.L. Phillips, P.D. Bristowe, Experimental and modelling techniques for assessing the adhesion of very thin coating on glass, J. Phys. D Appl. Phys. 42 (2009) 214003–214014.
[51] L. Zhang, T. Ohmura, K. Sekido, T. Hara, K. Nakajima, K. Tsuzaki, Dislocation character transition and related mechanical response in a body-centered cubic single crystal, Scr. Mater. 67 (2012) 388–391.
[52] O.R. Fuente, J.A. Zimmerman, M.A. Gonzalez, J. Figuera, J.C. Hamilton, W.W. Pai, J.M. Rojo, Dislocation emission around nanoindentations on a (001) fcc metal surfaces studied by scanning tunneling microscopy and atomistic simulations, Phys. Rev. Lett. 88 (2002) 011–014.
[53] B. Li, P.C. Clapp, J.A. Rifkin, X.M. Zhang, Molecular dynamics simulation of stick-slip, J. Appl. Phys. 90 (2001) 3090–3094.
[54] Y. Shibutani, T. Tsuru, A. Koyama, Nanoplastic deformation of nanoindentation: crystallographic dependence of displacement bursts, Acta Mater. 55 (2007) 1813–1822.
[55] Q.H. Fang, L.C. Zhang, Prediction of the threshold load of dislocation emission in silicon during nanoscratching, Acta Mater. 61 (2013) 5469–5476.
[56] D. Ghosh, G. Subhash, R. Radhakrishnan, T.S. Sudarshan, Scratch-induced microplasticity and microcracking in zirconium diboride-silicon carbide composite, Acta Mater. 56 (2008) 3011–3022.